Describing coseismic groundwater level rise using tank model in volcanic aquifers, Kumamoto, southern Japan

Makoto Kagabu[1*], Kiyoshi Ide[2], Takahiro Hosono[3], Kei Nakagawa[1], Jun Shimada[3]

1: Faculty of Environmental Science, Nagasaki University, 1-14 Bunkyo-machi, 852-8521, Japan

2: Department of Regional Environment System, Shibaura Institute of Technology, Japan

3: Faculty of Advanced Science and Technology, Kumamoto University, Kurokami 2-39-1, Kumamoto 860-8555, Japan

* Corresponding author (Makoto Kagabu: kagabu@nagasaki-u.ac.jp)

Abstract

The change of groundwater levels after the 2016 M_w 7.0 Kumamoto crustal earthquake was evaluated using a simple conceptual hydrological model in an attempt to show the presence, intensity, and probable mechanism of water level rise observed in Kumamoto where a comprehensive observation-well network exists. A tank model was applied to verify 16 wells in the study field. In the model groundwater levels were first calibrated for the periods in ca. 2 years before the main shock using several hydrological parameters including precipitation, evapotranspiration, water recharge and discharge, and artificial recharge by irrigation. Water levels were then simulated by extrapolating this law of water fluctuating patterns for ca. 2.5 years after the main shock of the earthquake, without considering hydrogeological changes due to the earthquake. A difference in groundwater levels between observation and simulation results yields a degree of coseismic water level rises for each well. The coseismic abnormal water level increase was calculated to be ~11 m in 4 to 5 month after the main shock and was most significantly on the western slope of the Aso caldera rim mountains. The spatial distribution of the coseismic water increases clarified that the most dominate increasing anomalies

prevail at mountain feet surrounding the plains, suggesting the occurrence of coseismic mountain water release resulting in the rise of water levels in downslope aquifers. Identified coseismic water level increases still continue up to 2.5 years after the earthquake, probably because changes in hydrogeological properties in mountain aquifers, i.e., permeability, are still sustained. Our forecasting water recovering trends require ca. 3.5 to 5 year after the earthquake for complete recovery to the original conditions. We demonstrated that our approaches are capable of describing coseismic water level changes and could potentially be applied to other fields.

Keywords: *earthquake; groundwater level change, tank model, Kumamoto*

1. Introduction

Groundwater comprises 96% of the Earth's unfrozen freshwater (Shiklomanov and Rodda, 2003) and is important for drinking water resources, feeding springs and streams, and maintaining natural marine ecosystems through submarine discharge. In the Kumamoto area, located in the central part of Kyushu Islands, southwest Japan (Fig. 1), ca. 1 million people in and around this area depend entirely on groundwater for drinking purposes, consisting the largest groundwater user areas in Japan. Because groundwater is a fundamentally important resource for Kumamoto citizens, both national and local governments have installed many observation wells (Fig. 1), and they put an effort to maintain operations and protection for sustainable use of these resources over the past few decades (e.g., introduced by Taniguchi et al., 2019). Therefore, describing the coseismic hydrological changes which occurred after the 2016 M_w 7.0 Kumamoto earthquake (Hosono et al., 2019) is important issue to address.

The presence of hydrological changes in response to large earthquakes have been documented.

These changes have been confirmed from field observations, i.e., an increased spring discharge, appearance of new springs, groundwater level changes in wells both for near and far fields (e.g., Rojstaczer and Wolf, 1992; Muir -Wood and King, 1993; Brodsky et al., 2003). Groundwater level changes caused by crustal stress changes have been documented for nearly 50 years (e.g., Bredehoeft et al., 1965; Roeloffs, 1998) and detailed changing processes and mechanisms are reported more frequently for couple of decades, with a greater availability of high-frequency water level records (Brodsky et al., 2003; Roeloffs and Quilty, 1997; Roeloffs et al., 2003; Weingarten and Ge, 2014; Liu et al., 2018). Another important coseismic hydrological change mechanism invoked is aquifer permeability changes due to strong seismic vibrations and structural deformations (Reasenberg, 1999; Chen et al., 2015; Barberio et al., 2017), which hydrological response have been recognized most frequently from increasing water discharges (e.g., Manga et al, 2003; Wang et al., 2004; Sato et al., 2000) and groundwater level rise in wells (Amoruso et al., 2011; Cox et al., 2012). However, few studies have investigated these phenomena and more studies using a greater number of springs and wells are required to investigate and to increase global understanding of this issue (Rosen et al., 2018).

The 2016 Kumamoto crustal earthquake sequence started with a M_w 6.2 fore shock on 21:26 JST at April 14, 2016, followed by many aftershocks. These are strike-slip and normal displacement of the active Futagawa and Hinagu faults with focal depths of 3–17 km (e.g., Sano et al., 2016). Among these aftershocks the largest one (M_w 7.0) hit on 1:25 JST at April 16, 2016 that we call it as the “main shock” (e.g., Kato et al., 2016). This disaster caused 273 fatalities and more than 8,500 houses completely collapsed (Fire and Disaster Management Agency, 2016). The main shock reveals new surface ruptures and faults around the Ezu Lake, Mt. Kinpo, northwest of Aso caldera rim mountains, and northeast of Aso caldera (see Fig. 1; Fujiwara et al., 2016). The preliminary research on coseismic hydrological changes mechanism (Hosono et al., 2019) revealed that the groundwater level dropped immediately after the main shock due to water drawdown through rupture systems around the Suizenji fault zone.

They also identified water level increase after this initial groundwater drop most prominently at eastern recharge areas and invoked it to be caused by coseismic mountain water release due to permeability enhancement (Jónsson et al., 2003; Wang et al., 2004; Wang and Manga, 2015). However, the observed water rise has not yet been evaluated considering long-term hydrological influences such as precipitation, evapotranspiration, infiltration, and discharges, that can also cause water level changes, and thus, coseismic water level rise has not yet been defined or characterized.

Except data-driven soft computing approaches such as Prophet algorithm (Matsumoto et al., 2003) and Support Vector Machine (Wang et al., 2019), application of hydrological-parameters-involved water flow simulation model can be a clue to more accurately distinguish coseismic changes from water level changes owing to local hydrological cycle. We can assume that these simulated values, without considering seismic effect, allow for comparison with observation data and for characterization of the presence, intensity, and distribution of coseismic effects more accurately. Among many hydrological simulators developed and applied (Brodsky et al., 2003; Nespoli et al., 2016), the tank model (Sugawara, 1979) is known as a simple but useful (and minimum cost) conceptual hydrological model capable to simulate different system states without considering complex hydrogeological structure (Lee et al., 2005; Hong et al., 2015; Aqili et al., 2018). We assume that if we can develop well-reproduced water level fluctuations for the period before the earthquake and if we can extend the same law for post-earthquake period, the results of this simulation can be used to compare with observation data to extract coseismic change signals only. Calculated coseismic change data are further used to discuss for their spatial variations, probable cause of water level rise, and future prospective. Although the tank model has not been frequently used for evaluating coseismic hydrological change, we propose this approach is applicable and is the one of simplest and easiest way to address the issue raised.

2. Study area

The Kumamoto area is characterized hydrologically by active groundwater flows within Quaternary volcanic pyroclastic deposits, porous lava, and alluvial deposits. Two major aquifer systems are separated by an impermeable aquitard, with an unconfined aquifer (ca. < 50 m deep, we call it as "first aquifer") overlying a confined to semi-confined aquifer (ca. 60–200 m, we call it as "second aquifer"). The active groundwater flow systems in the Kumamoto area are characterized by a highly permeable hydrogeology, a steep hydraulic gradient of the volcanic pyroclastic flow, and a large amount of precipitation (https://weather.time-j.net/Climate/Chart/Kumamoto). The major water resources in the area are dependent on the groundwater intake from the second aquifer. A number of studies have revealed detailed groundwater environments including groundwater flow systems (Kosaka, 2002), water quality (Hosono et al., 2013; Hossain et al., 2016; Zeng et al., 2016), soil water downward transportation (Okumura et al., 2018), and groundwater residence time (Kagabu et al., 2017).

Groundwater flow systems are well understood within the study area based on long-term groundwater level monitoring and groundwater modeling. The most significant groundwater flow system of the second aquifer is the flow from mid-stream area of the Shirakawa River toward the discharge area of the Ezu Lake with discharge rate of 1.5×10^8 m^3 y^{-1}. The Aso caldera rim mountains are considered major recharge area of this regional main groundwater flow system (Shimada et al., 2012).

In total 113 observation wells are installed in the Kumamoto area which are operated by different agencies (Kumamoto Prefectural, Kumamoto City, Water and Sewerage Bureau, and Ministry of Land, Infrastructure, Transport and Tourism) for monitoring and management of drinking water resources. The longest groundwater level records extend for more than 35 years. All groundwater level data were

121 collected and compiled in this study. Among 113 wells, 21 monitoring wells were not used as data
122 sources because of direct mechanical damage and data loss caused by the earthquake, leaving useful
123 data from 94 wells at 72 locations. Multiple wells with different depths are located at the same site
124 (Fig. 1): 28 and 66 wells for the first and second aquifers, respectively. Groundwater levels are
125 recorded with a pressure sensor and archived hourly as digital data. All data used to illustrate map and
126 figures are provided in Supplementary Table S1.
127
128 **3. Observed groundwater level data**
129
130 3.1. Monthly groundwater level fluctuation
131
132 Fig. 2 shows the monthly average groundwater level fluctuation for five years for several
133 representative observation wells from the study area. The figure shows water level fluctuation is
134 relatively small near coastal areas, while larger seasonal variations are observed in eastern recharge
135 areas. Within the annual hydrological cycle, water levels are the highest in summer (June–October)
136 and lowest in winter (January–April), respectively. In addition, the water level increases sharply at the
137 period when huge precipitation occurred. The observed water level peak in summer time is attributed
138 not only to heavy rainfall but also to the influence of irrigation water in paddy fields except for western
139 coastal areas (Shimada et al., 2012). In contrast, water levels become lowest when paddy fields are
140 not irrigated out of rainy season.
141
142 3.2. Daily groundwater level fluctuation
143
144 The Kumamoto earthquake occurred in April 2016. Usually, April is the time of lowest water

145 level throughout the year in the Kumamoto area (Fig. 2). To precisely examine the groundwater level
146 fluctuations during before and after the earthquake (from April 2014 till November 2018), daily
147 average water level time series is depicted for 3 observation wells located in the eastern recharge areas
148 (Fig. 3, wells D, F, and J).

149 The vertical green lines in the figure represent April at each year (showed for reference of the
150 same month when the earthquake occurred). It is clear from this figure that the increase in water levels
151 from the lowest level started from April in 2016, almost immediately after the earthquake, whereas
152 seasonal water level rise generally starts from mid-June for the other years (2014, 2015, 2017, and
153 2018). Furthermore, the peak of the water level around September and October in 2016 was several
154 meters higher than the water levels observed during the 2 years before the earthquake. Similarly, the
155 water levels in April in the next year (2017) after the earthquake showed considerably higher value
156 than the lowest water level found in the year 2015. These observations imply that the water level rise
157 started immediately after the earthquake and this is still continued after at least 1 year of the main
158 shock, which should be examined using the hydrological simulations proposed in this study.

159

160 3.3. Spatial distribution of groundwater level changes

161

162 The differences in the groundwater levels of the second aquifer before and after the earthquake
163 are mapped (Fig. 4) to ascertain spatial groundwater level changes in the Kumamoto area. It is shown
164 in this map that the groundwater levels dropped near Ezu Lake immediately after the earthquake (Fig.
165 4a). Hosono et al. (2019) has recently described detailed mechanism of this phenomenon. However,
166 at 1 month after the main shock (Fig. 4b), a water level rose on the western foot of Aso caldera rim
167 mountains. Furthermore, water level increases of 10 m or more were observed on the western slope of
168 Aso caldera rim mountains 5.5 months after the earthquake (Fig. 4d). These water level increases were

less obvious in the plain.

These results show a large increase in the groundwater levels after the earthquake was most dominantly presented in the western slope of the Aso caldera rim mountains. This tendency is obvious that the closer point to the Aso caldera rim mountains has larger increase levels.

4. Methods

4.1. Traditional tank model

To evaluate coseismic water level rise after the main shock of the 2016 Kumamoto earthquake, a tank model was adopted to reproduce groundwater level fractionations considering local hydrological cycles. After tuning and calibrating parameters and confirming model performance in reproducing water level fractionations before the main shock (from April 1, 2014 until April 15, 2016), the same parameters were used to calculate groundwater levels after the main shock (from April 16, 2016 until November 30, 2018). Then, a difference between the observed and calculated (simulated) water levels was obtained which can be attributable to coseismic effect (in this paper we expressed this value as an "abnormal water rise", see Discussion).

The tank model is applied in this study. This model was proposed by Sugawara (1979) to perform river runoff analyses using a simple hydrological concept. This model can also be useful to assess groundwater level fractionations with respect to a specific well (Hong et al., 2015; Kiriyama et al., 2000). The model assumes some tanks (storage) and holes that water can flow-in and -out to numerically explain water balance in the target field (Fig.5). This expresses nonlinear phenomenon with complex water transportation and interaction behaviors across different water bodies including river discharge variability and groundwater level fractionation due to rain falls in the target catchment.

193 The traditional tank model is based on the assumption that precipitation infiltration and runoff
194 are the principle functions affecting water storage in the basin and storage can be expressed by
195 hypothesizing several parallel and tandem tanks (Fig. 5). Outlet holes on the side of each tank represent
196 outflows. The outflow flux from the holes is set as proportional to the tank depth. The tank model has
197 a simple structure, but it does not impair the physical meaning of the rainfall-runoff processes and
198 water uptake. It can represent nonlinearity of the runoff phenomenon and accurately estimate
199 discharges if the model parameters are well defined. The number and arrangement of tanks are set
200 according to the runoff characteristics of the target basin. A greater number of tanks gives better
201 response to runoff variations. However, it is desirable to try adaptation with as few tanks as possible
202 to reduce complexity.
203
204 4.2. Constructed tank model for reproducing groundwater level fluctuations
205
206 As mentioned earlier, the aquifer structure of the Kumamoto area comprises the first aquifer in
207 the shallow layer and the second aquifer in the deep layer. Considering the presence of the upper
208 unsaturated zone, a three-stage tank model was constructed (Fig. 5). The first to third tanks express
209 the hydrological processes in unsaturated zone, first aquifer, and second aquifer, respectively.
210 The tank model adopted for this study has 8 parameters to be determined (Z_1, Z_2, Z_3, α_1, α_2, β_1,
211 β_2 and γ_1). In addition, the initial depths must be set for each tank (H_1, H_2, and H_3) and thus the total
212 unknown parameters are 11.
213 In Fig. 5, Z_1, Z_2 and Z_3 represent the height of the upper hole of the first tank, lower hole of the
214 first tank and upper hole of the second tank, respectively. An upper hole of the first tanks (Q_2)
215 represents the surface runoff, which does not flow into next stage tanks. The height Z_2 corresponds to
216 the storage effect in the first tank. An upper hole above of the second tank (Q_3) assumes a bypass flow

directly flowing into the third tank when water exceeds the height of the upper hole (Z_3). Consequently, the groundwater levels rise sharply following heavy precipitation.

On the first day of the tank model calculation, the observed groundwater level was given to the water depth of the third tank (H_3). Arbitrary values were given to other tanks as an initial value, and calculation was started. If the observed groundwater level responds quickly to the heavy rain, the distance to the upper hole of the second tank (Z_3) was shortened and/or the volume of bypass flow (Q_3) was increased by regulating the coefficient β_1. The groundwater level fluctuation is small at the observation wells located in the coastal area. At such points, each coefficient value is relatively small so that the calculated groundwater level does not fluctuate greatly. The runoff water from the third tank (Q_5) is adjusted to reproduce water level H_3.

In this study, since the analysis target of the tank model is the groundwater level of the second aquifer, the water depth H of the third tank (H_3) can be regarded as the groundwater level. Best matching parameters are sought by trial and error to reproduce observed groundwater level for each well. The unit of depth (H_1 to H_3) and height (Z_1 to Z_3) is mm, and outflow (Q_1 to Q_5) is mm / day.

Now the water depth S at the day i for the first tank S_1 can be express as following equation

$$S_1(i)=S'_1(i-1)+P(i)-E(i)\ldots(1)$$

where $S'(i\text{-}1)$, P, and E represent depth of prior day, precipitation, and evapotranspiration, respectively. Then, outflow Q for the first tank Q_1 and Q_2 can be determined as

$$Q_1(i)=\alpha_1 I[S_1(i)-Z_2]\ldots(2) \text{ and}$$

$$Q_2(i)=\alpha_2 I[S_1(i)-Z_1]\ldots(3), \text{ respectively,}$$

where α_1 and α_2 represent hole coefficients for the first tank of lower and upper holes, respectively (Fig. 5). The I indicates a function such that $I[x] = x$ when $x > 0$, and $I[x] = 0$ when $x \leq 0$. Here, the water depth for the first tank H_1 can express by the following equation,

$$H_1(i) = S_1(i) - Q_1(i) - Q_2(i) \quad \ldots(4)$$

The same calculation can be performed using outflow and inflow into the second and third tanks as following equations:

$$H_2(i) = H_2(i-1) + Q_1(i) - Q_3(i) - Q_4(i) \ldots(5)$$

$$H_3(i) = H_3(i-1) + Q_3(i) + Q_4(i) - Q_5(i) \ldots(6)$$

Here, the outflow Q for the second tank Q_3 and Q_4 and for the third tank Q_5 can be determined as

$$Q_3(i) = \beta_1 I[H_2(i) - Z_3] \ldots(7),$$

$$Q_4(i) = \beta_2 \times H_2 \ldots(8),$$

$$Q_5(i) = \gamma_1 \times H_3 \ldots(9), \text{ respectively.}$$

The amount of precipitation P represents the daily precipitation observed at the Kumamoto Meteorological Observatory (http://www.data.jma.go.jp/obd/stats/etrn/index.php). Evapotranspiration E was estimated using the Thornthwaite method (Thornthwaite, 1948), which is calculated as a function of the mean monthly temperature (temperature data source: http://www.data.jma.go.jp/obd/stats/etrn/view/nml_sfc_ym.php?prec_no=86&block_no=47819). To maintain water balance throughout the tank systems the loss of water by evapotranspiration was

considered from the second or third tank when the upper tanks are empty.

Above calculations were repeated from April 1, 2014 until April 15, 2016. We started calculations using a three-stage tank. However, the test results demonstrate the necessity of considering paddy irrigation to reproduce large water level changes in summer. Therefore, an additional tank (paddy tank) was set during May–November to reproduce the groundwater recharge from paddy irrigation (see Fig. 5), as has been argued by previous researchers (Kiriyama et al., 2000).

The inflow for the paddy tank was determined by the residual amount of precipitation (P) and evapotranspiration (E). A factor (ε: 0 to 1) was set for each well to regulate this inflow amount. The outflow for the paddy tank (Q_6: mm / day) can be determined as

$$Q_6(i) = \gamma_2 \times H_4 \ldots (10)$$

After the main shock of the 2016 Kumamoto earthquake sequence (April 16, 2016), water level simulation was performed using parameters set up for each well reproducing hydrological data during the 2 years before the earthquake and reported precipitation amount with the same data source and evapotranspiration calculated with the same way described above. A set of calculations was conducted for 16 representative observation wells over the Kumamoto area, especially at the eastern recharge area where a significant water level rise was reported after the earthquake (Hosono et al., 2019). We evaluated whether these groundwater level rises can be explained by seasonal hydrological variabilities or whether they are a result of the earthquake using constructed tank model.

5. Results and discussion

289 5.1. Estimation on decrease in groundwater recharge by paddy irrigation

290

291 For the tank model analysis, we considered the reduction of paddy field irrigation caused by the
292 earthquake. Because of the earthquake and water leakage caused by earthquake fractures that occurred
293 in the paddy field area, some paddy fields could not be irrigated because of damage to the irrigation
294 channels. Therefore, groundwater recharge from paddy fields was reported to decrease considerably
295 after the earthquake (Ichikawa, 2018).

296 Annual groundwater recharge exceeding 60 million m^3 was estimated according to changes in the
297 estimated value of groundwater recharge from paddy fields in the middle basin of the Shirakawa River
298 by Ichikawa (2018) as inferred from changes that occurred during 2004–2017 (Fig. 6). However, the
299 recharge amount was less than 30 million m^3 in 2016 after the earthquake: about 54% lower. The
300 groundwater recharge amount was estimated to have decreased by about 10% in 2017. The recharge
301 amount from the additional paddy tank (outflow hole Q_6 in Fig. 5) decreased by narrowing the runoff
302 restriction parameter (γ_2) from the pre-seismic value (2016, 46%; 2017, 90%). Therefore, we inferred
303 the paddy field irrigation reduction as earthquake-associated.

304

305 5.2. Tank model reproducibility

306

307 Figure 7 shows the scatter plot for the observed versus simulated groundwater level for 16 wells.
308 In the two years preceding the earthquake, the value calculated by the tank model and the observed
309 value in any observation well plotted almost 1:1 line with high correlation coefficient. Consequently,
310 the reproducibility by the tank model is high. However, the correlation coefficient was slightly lower
311 for the wells located in the plain to coastal area compared to other points. This may due to the small
312 annual groundwater level fluctuation.

313 The scatter plot deviates largely from the 1:1 line immediately after the earthquake in many
314 observation wells especially located in eastern areas (Fig. 7). An example of the daily groundwater
315 level fluctuation of observed and calculated by tank model is presented in Fig. 8. Results showed that
316 the observed groundwater level exhibited a markedly higher level after the earthquake. Especially, the
317 observation wells distributed around the western slope of Aso caldera rim mountains (Wells B and F
318 in Fig. 8).
319 Because the observed value was higher than the calculated value immediately after the earthquake,
320 it can be judged as the abnormal water level associated with the earthquake. However, in the
321 observation wells located at a distance from the western slope of Aso caldera rim mountains (Wells N
322 and P in Fig. 8), the difference between the simulated groundwater level by the tank model and the
323 observed water level after the earthquake is small. The abnormal water level is found only to a slight
324 degree in these wells.
325
326 5.3. Identification of the coseismic groundwater level rise
327
328 In the previous section, a huge gap was identified between the observed and simulated values after
329 the earthquake found in the wells located in the western slope of the caldera rim mountains. A
330 difference between the observed and simulated water levels was obtained which can be attributable to
331 coseismic effect. We defined this value as an “abnormal water rise”.
332 To identify the spatial and temporal distribution of this “abnormal water rise”, its distribution was
333 plotted as a circular spatial map, as shown in Fig. 9. Immediately after the earthquake, no significant
334 “abnormal water rise” is found, however, it increases with time especially in the area around the
335 western slope of Aso caldera rim mountains. The maximum difference was observed 4 to 5 months
336 after the earthquake, with a maximum difference of more than 10 m at the easternmost point of the

observation well network (Well A in Fig. 9e). Whereas, “abnormal water rise” is not found in the observation wells located at a distance from the western slope of Aso caldera rim mountains. The “abnormal water rise” generally decreases with time, but a difference of several meters is still seen in two years after the earthquake (Fig. 9h). About two and a half years after the earthquake, the value decreased considerably (Fig. 9i).

5.4. Evaluation of “abnormal water rise”

To quantitatively evaluate the degree of coseismic water revel rise, the "abnormal water supply index" shown below was defined. The method of calculation is explained using the water level fluctuation chart (Well F in Fig. 8). Immediately after the earthquake, the observed values show a sharp rise, but the simulated value without considering hydrogeological changes due to the earthquake, shows no increase at this point. In other words, the rise in the observed water level is regarded as attributable to the addition of new groundwater other than precipitation because of the earthquake (painted in pink in Fig. 8 of Well F).

The abnormal water level amount is evaluated by supplying water to compensate for the difference between observed and simulated values. Specifically, in the tank model configuration presented in Fig. 5, water is forcibly added to the third tank to match the actual measurement value. This additional input water volume is defined as the “abnormal water supply index.” The index calculation period is set to 3 months from the earthquake occurrence. The observed groundwater level (Fig. 3) shows a rising trend immediately after the earthquake, and its trend was further strengthened after 3 months. This further rising after 3 months seems to overlap with the usual timing of groundwater increasing (from the end of June to the beginning of July). Thus, it is considered that this further rising includes factors other than earthquakes. Therefore, we thought that it would be better to consider the impact of

361 the earthquake alone; the index calculation period set to 3 months.

362 The 3-month accumulated value to compensate groundwater level differences between the
363 observed and the calculated value is calculated. Then it is divided by 90 days, which is the “abnormal
364 water supply index” (mm/day).

365 This index was obtained for all observation well sites for which a tank model analysis was applied.
366 The amount is shown as a circular spatial distribution map, as shown in Fig. 10. This index was the
367 largest at Well A (80.1 mm / day) near the caldera rim mountains. Similarly, Wells B (69.7 mm / day),
368 C (63.0 mm / day), and D (59.3 mm / day) located at the western slope of caldera rim mountain area
369 are also large values. However, an abnormal water supply index was almost zero in the plane area
370 (Well M, N, and O). The groundwater supply causing an abnormal water level rise accompanying the
371 earthquake occurs mainly in the area around the western slope of Aso caldera rim mountains. Although
372 this value is not actually observed, it is possible to grasp the quantity of new groundwater supplied
373 after the earthquake, suggesting quite a large volume.

374

375 5.5. Possible mechanisms

376

377 Cases in which water was supplied accompanying large earthquakes were reported from several
378 earlier studies. The mechanisms differ among regions. Examples include the rise of pore water
379 pressure with liquefaction (Lai et al., 2004; Wang et al., 2001), falling of soil water in unsaturated zone
380 (Manga and Rowland, 2009; Mohr et al., 2017), the contribution of deep fluid (Sibson et al., 2003;
381 Tsunogai and Wakita, 1995), and the release of groundwater in the mountains (Wang and Manga, 2015;
382 Wang et al., 2004). Among the mechanisms proposed in those earlier studies, the mechanism with the
383 most likelihood of raising the groundwater level near Aso caldera rim mountains, as observed in this
384 study, is the release of groundwater in the mountains.

385 The mountain groundwater release mechanism is explained by the formation of the fractures during
386 the earthquake. The earthquake breached the impervious aquifer and greatly enhanced the vertical
387 permeability, allowing rapid downward draining of water to recharge underlying aquifers (Wang et al.,
388 2004). This previous study observed a temporary increase (within few weeks) of “surface water”
389 discharge after the earthquake. In the case of the Kumamoto earthquake, the river water discharge
390 increased after the earthquake were also observed (Hosono et al., 2019). On the other hand, our
391 research captures the change of the “groundwater” level, of which fluctuation is not as sharp compared
392 to the surface water. However, the phenomenon itself is considered to be a mechanism that is in good
393 agreement with previous studies that discussed the release of mountain groundwater by these
394 earthquakes. For the Kumamoto area, in fact, Fujiwara et al. (2016) reported that a fracture zone was
395 newly formed in the Aso caldera rim mountains because of the 2016 Kumamoto earthquakes. A
396 hydrogeological cross-section diagram from east to west in the Kumamoto area that includes this
397 newly formed fracture zone is shown in Fig. 11. It is clear that there is a positional relationship where
398 the release of mountain groundwater occurred. Considering the Kumamoto earthquake, especially near
399 the caldera rim mountains, points at which the groundwater level rose remarkably after the earthquake
400 are concentrated.
401 Furthermore, the previous studies have suggested that the variability of permeability over time may
402 be caused by fracture depressurization (Faoro et al., 2012) or controlled by geochemical processes that
403 can slowly clog the flow path (Manga et al., 2012; Candela et al., 2014). The fact that the “abnormal
404 water rise” is decreasing with time (Fig. 9) means that the permeability increased immediately after
405 the earthquake gradually decreased due to the mechanism such that clogging of the flow path.
406 Therefore, the groundwater stored in the mountain aquifer of caldera rim mountains is released and
407 is supplied to downstream areas, which is the likely mechanism.
408

409 5.6. Future prospective

410 Because the durations of such abnormal water levels differ depending on the location, the durations
411 of the difference between the observed value and the calculated value in each observation well are
412 presented in Fig. 12. According to this figure, because the water level difference was within ±1 m
413 before the earthquake, the observed values can almost be reproduced at each location. However
414 deviations were found at many points immediately after the earthquake, in the observation wells of A,
415 B, C, D, E, F, G, and H. Even at the end of November 2018, when two and a half years had passed
416 since the earthquake, a gap separates the calculated and observed values. Although the groundwater
417 level difference continued until 2017, it shrank gradually by 2018. At the end of 2018, it shrank to
418 about 4 m at the largest point. The groundwater level difference between the simulated and the
419 observed value tends to shrink gradually with time, suggesting that it is gradually returning to normal.
420 The future progress of the water level fluctuation must be monitored carefully. The area with the
421 greatest groundwater level difference is at the western slope of Aso caldera rim mountains. However,
422 abnormal water levels were only slightly recognized at points distant from there.

423 Here, we examined when the “abnormal water rise” would over. Because in the case of this study,
424 coseismic increase of groundwater level are relatively long term compared to previous studies, usually
425 it sustains from a few days to several months (Montgomery and Manga 2003). The regression line in
426 polynomial curve of the water level reduction trend was obtained from August 2016 to the end of
427 November 2018, and we defined the day when the intersection point of the regression curve with the
428 X axis as the end date of “abnormal water rise”.

429 The end date of abnormal water rise in each well was calculated and summarized in Table 1. In Fig.
430 12, two regression curves of the water level are shown whose inter section period was the closest (Well
431 E: November, 2019) and remotest (Well A: March, 2021) from the earthquake, namely the “abnormal
432 water rise” will be shrunken ca. 3.5 to 5 years after the earthquake. If the clogging accelerates, the

abnormal water level will be reduced faster.

6. Conclusions

A three-stage tank model was developed to simulate water level fluctuations within the aquifer structure of the Kumamoto area. The water fluctuations that would have occurred in the absence of the earthquake effects were simulated by extrapolating the patterns observed in the period ca. 2 years before the earthquake. The simulated water levels were compared with observed data following the earthquake to extract the coseismic change signals only. Application of the tank model successfully identified abnormal water supply from the mountains to regional groundwater systems. This was most significant at the western slope of the Aso caldera rim mountains that peaked at about 4 to 5 months after the earthquake. This was most reasonably explained by coseismic mountain water release due to permeability enhancement. After the maximum increase in water levels due to addition of this new water, the water levels tend to decrease probably owing to permeability recovery to original conditions by clogging. Our simple estimation suggests this abnormal groundwater level rise will be reduced in 3.5 to 5 years after the earthquake. These retention times may reflect multiple factors including an intensity of seismic deformations, storage capacity and properties of mountain aquifers and local precipitation amounts. The spatial and temporal variation of abnormal water supply would be fully proved based on isotopic fingerprinting approach using dataset from high-time-resolution water sampling campaigns before and after the earthquake. However, in the absence of such high resolution data, the tank model allowed the abnormal water level rise to be identified.

Acknowledgments

Authors thank the research group of Japanese Association of Groundwater Hydrology for fruitful discussion. Also, authors thank H. Sleight who is a native speaker of English for the advice to improve the text. This study was financially supported by SUNTORY Kumamoto groundwater research project.

References

Amoruso, A., Crescentini, L., Petitta, M., Rusi, S., Tallini, M., 2011. Impact of the 6 April 2009 L'Aquila earthquake on groundwater flow in the Gran Sasso carbonate aquifer, Central Italy. Hydrological Processes, 25(11): 1754-1764. DOI:10.1002/hyp.7933

Aqili, S.W., Hong, N., Hama, T., Suenaga, Y., Kawagoshi, Y., 2016. Application of Modified Tank Model to Simulate Groundwater Level Fluctuations in Kabul Basin, Afghanistan. Journal of Water and Environment Technology, 14(2): 57-66. DOI:10.2965/jwet.15-039

Barberio, M.D., Barbieri, M., Billi, A., Doglioni, C., Petitta, M., 2017. Hydrogeochemical changes before and during the 2016 Amatrice-Norcia seismic sequence (central Italy). Scientific Reports, 7(1): 11735. DOI:10.1038/s41598-017-11990-8

Bredehoeft, J.D., 1967. Response of well-aquifer systems to Earth tides. Journal of Geophysical Research (1896-1977), 72(12): 3075-3087. DOI:10.1029/JZ072i012p03075

Brodsky, E.E., 2003. A mechanism for sustained groundwater pressure changes induced by distant earthquakes. Journal of Geophysical Research, 108(B8). DOI:10.1029/2002jb002321

Brodsky, E.E., Roeloffs, E., Woodcock, D., Gall, I., Manga, M., 2003. A mechanism for sustained groundwater pressure changes induced by distant earthquakes. Journal of Geophysical Research: Solid Earth, 108(B8). DOI:10.1029/2002jb002321

Chen, C.-H. et al., 2015. Groundwater–strain coupling before the 1999 M w 7.6 Taiwan Chi-Chi earthquake. Journal of Hydrology, 524: 378-384. DOI:10.1016/j.jhydrol.2015.03.006

Cox, S.C. et al., 2012. Hydrological effects of the M W 7.1 Darfield (Canterbury) earthquake, 4

September 2010, New Zealand. New Zealand Journal of Geology and Geophysics, 55(3): 231-247. DOI:10.1080/00288306.2012.680474

Fujiwara, S. et al., 2016. Small-displacement linear surface ruptures of the 2016 Kumamoto earthquake sequence detected by ALOS-2 SAR interferometry. Earth, Planets and Space, 68(1). DOI:10.1186/s40623-016-0534-x

Hong, N. et al., 2015. Simulation of Groundwater Levels Using Tank Model with Consideration of Mixed Hydrological Structure in Kumamoto City. Journal of Water and Environment Technology, 13(4): 313-324. DOI:10.2965/jwet.2015.313

Hosono, T. et al., 2013. The use of $\delta^{15}N$ and $\delta^{18}O$ tracers with an understanding of groundwater flow dynamics for evaluating the origins and attenuation mechanisms of nitrate pollution. Water Res, 47(8): 2661-75. DOI:10.1016/j.watres.2013.02.020

Hosono, T., Yamada, C., Shibata, T., Tawara, Y., Wang, C.Y., Manga, M., Rahman, A.T.M.S., Shimada, J., 2019. Coseismic groundwater drawdown along crustal ruptures during the 2016 Mw 7.0 Kumamoto earthquake. Water Resources Research, 55(7), 5891-5903.

Hossain, S., Hosono, T., Ide, K., Matsunaga, M., Shimada, J., 2016. Redox processes and occurrence of arsenic in a volcanic aquifer system of Kumamoto Area, Japan. Environmental Earth Sciences, 75(9). DOI:10.1007/s12665-016-5557-x

Ichikawa, T., Nakagawa, K., 2018. Impact of the 2016 Kumamoto earthquake on the recharge project in the middle area of Shirakawa River watershed. Abstract FP-113 presented at IAH 2018 Congress, Daejeon, Korea, 9-14 Sept.

Jónsson, S., Segall, P., Pedersen, R., & Björnsson, G. (2003) Post-earthquake ground movements correlated to pore-pressure transients. Nature, 424, 179-183. doi:10.1038/nature01776

Kagabu, M., Matsunaga, M., Ide, K., Momoshima, N., Shimada, J., 2017. Groundwater age determination using ^{85}Kr and multiple age tracers (SF_6, CFCs, and ^{3}H) to elucidate regional

groundwater flow systems. Journal of Hydrology: Regional Studies, 12: 165-180. DOI:10.1016/j.ejrh.2017.05.003

Kato, A., Nakamura, K., Hiyama, Y., 2016. The 2016 Kumamoto earthquake sequence. Proc Jpn Acad Ser B Phys Biol Sci, 92(8): 358-371. DOI:10.2183/pjab.92.359

Kiriyama, T., Ichikawa, T., Hoshida, Y., 2000. Conjecture of Groundwater Level using Tank Model in Kumamoto Area. PROCEEDINGS OF HYDRAULIC ENGINEERING, 44: 223-228. DOI:10.2208/prohe.44.223

Kosaka, H., Shimada. J. and Yamauchi, I., 2001. The groundwater flow system in the Kumamoto area by using a stable isotope ratio. Proc. of Annual meeting of Japanese Association of Groundwater Hydrology: 40-43.

Lai, W.-C. et al., 2004. Effects of seismic ground motion and geological setting on the coseismic groundwater level changes caused by the 1999 Chi-Chi earthquake, Taiwan. Earth, Planets and Space, 56(9): 873-880. DOI:10.1186/bf03352534

Lee, Y.H., Singh, V.P., 2005. Tank Model for Sediment Yield. Water Resources Management, 19(4): 349-362. DOI:10.1007/s11269-005-7998-y

Liu, C.-Y., Chia, Y., Chuang, P.-Y., Chiu, Y.-C., Tseng, T.-L., 2017. Impacts of hydrogeological characteristics on groundwater-level changes induced by earthquakes. Hydrogeology Journal, 26(2): 451-465. DOI:10.1007/s10040-017-1684-z

Manga, M., Brodsky, E.E., Boone, M., 2003. Response of streamflow to multiple earthquakes. Geophysical Research Letters, 30(5): n/a-n/a. DOI:10.1029/2002gl016618

Manga, M., Rowland, J.C., 2009. Response of Alum Rock springs to the October 30, 2007 Alum Rock earthquake and implications for the origin of increased discharge after earthquakes. Geofluids, 9(3): 237-250. DOI:10.1111/j.1468-8123.2009.00250.x

Matsumoto, N., Roeloffs, E.A., 2003. Hydrological response to earthquakes in the Haibara well,

528 central Japan – II. Possible mechanism inferred from time-varying hydraulic properties.
529 Geophysical Journal International, 155(3): 899-913. DOI:10.1111/j.1365-246X.2003.02104.x
530 Mohr, C.H., Manga, M., Wang, C.-Y., Korup, O., 2017. Regional changes in streamflow after a
531 megathrust earthquake. Earth and Planetary Science Letters, 458: 418-428.
532 DOI:10.1016/j.epsl.2016.11.013
533 Muir-Wood, R., King, G.C.P., 1993. Hydrological signatures of earthquake strain. Journal of
534 Geophysical Research: Solid Earth, 98(B12): 22035-22068. DOI:10.1029/93jb02219
535 Okumura, A., Hosono, T., Boateng, D., Shimada, J., 2018. Evaluations of the downward velocity of
536 soil water movement in the unsaturated zone in a groundwater recharge area using δ18 O tracer:
537 the Kumamoto region, southern Japan. Geologia Croatica, 71(2): 65-82.
538 DOI:10.4154/gc.2018.09
539 Quilty, E.G., Roeloffs, E.A., 1997. Water-level changes in response to the 20 December 1994
540 earthquake near Parkfield, California. Bulletin of the Seismological Society of America, 87(2):
541 310-317.
542 Reasenberg, P.A., 1999. Foreshock occurrence before large earthquakes. Journal of Geophysical
543 Research: Solid Earth, 104(B3): 4755-4768. DOI:10.1029/1998jb900089
544 Roeloffs, E. et al., 2011. Groundwater-Level Changes Caused by Strain and Seismic Shaking from the
545 August 23, 2011 Mw5.8 Virginia Earthquake. Abstract S14B-07 presented at 2011 Fall Meeting,
546 AGU, San Francisco, Calif., 5–9 Dec.
547 Roeloffs, E., Quilty, E., Scholtz, C.H., 1997. Case 21 water level and strain changes preceding and
548 following the August 4, 1985 Kettleman Hills, California, earthquake. pure and applied
549 geophysics, 149(1): 21-60. DOI:10.1007/bf00945160
550 Roeloffs, E. et al., 2003. Water-level changes induced by local and distant earthquakes at Long Valley
551 caldera, California. Journal of Volcanology and Geothermal Research, 127(3-4): 269-303.

552 DOI:10.1016/s0377-0273(03)00173-2
553 Roeloffs, E.A., 1998. Persistent water level changes in a well near Parkfield, California, due to local
554 and distant earthquakes. Journal of Geophysical Research: Solid Earth, 103(B1): 869-889.
555 DOI:10.1029/97jb02335
556 Rojstaczer, S., Wolf, S., 1992. Permeability changes associated with large earthquakes: An example
557 from Loma Prieta, California. Geology, 20(3): 211-214. DOI:10.1130/0091-
558 7613(1992)020<0211:pcawle>2.3.co;2
559 Rosen, M.R. et al., 2018. Mechanisms of Earthquake-Induced Chemical and Fluid Transport to
560 Carbonate Groundwater Springs After Earthquakes. Water Resources Research, 54(8): 5225-
561 5244. DOI:10.1029/2017wr022097
562 Sato, T., Sakai, R., Furuya, K., Kodama, T., 2000. Coseismic spring flow changes associated with the
563 1995 Kobe Earthquake. Geophysical Research Letters, 27(8): 1219-1222.
564 DOI:10.1029/1999gl011187
565 Shiklomanov, I.A., and J.C. Rodda, 2003. World water resources at the beginning of the 21st century.
566 Cambridge University Press, Cambridge.
567 Shimada, J., Ichiyanagi, K., Kagabu, M., Saita, S., Mori, K., 2012. Effect of Artificial Recharge Using
568 Abandoned Rice Paddies for Sustainable Groundwater Management in Kumamoto, Japan, 59-69
569 pp. DOI:10.1061/9780784412312.007
570 Sibson, R.H., Rowland, J.V., 2003. Stress, fluid pressure and structural permeability in seismogenic
571 crust, North Island, New Zealand. Geophysical Journal International, 154(2): 584-594.
572 DOI:10.1046/j.1365-246X.2003.01965.x
573 Sugawara, M., 1979. Automatic calibration of the tank model Hydrological Sciences Bulletin, 24(3):
574 375-388. DOI:10.1080/02626667909491876
575 Taniguchi, M., Burnett, K., Shimada, J., Hosono, T., Wada, C.A., Ide, K., 2019. Recovery of lost nexus

576 synergy via payment for environmental services in Kumamoto, Japan. Front. Environ. Sci. 7, 28.
577 Thornthwaite, C.W., 1948. An approach toward a rational classification of climate. Geogr. Rev., 38:
578 55-94.
579 Tsunogai, U., Wakita, H., 1995. Precursory Chemical Changes in Ground Water: Kobe Earthquake,
580 Japan. Science, 269(5220): 61-63. DOI:10.1126/science.269.5220.61
581 Wang, C.-y., Cheng, L.-H., Chin, C.-V., Yu, S.-B., 2001. Coseismic hydrologic response of an alluvial
582 fan to the 1999 Chi-Chi earthquake, Taiwan. Geology, 29(9): 831-834. DOI:10.1130/0091-
583 7613(2001)029<0831:chroaa>2.0.co;2
584 Wang, C.-Y., Manga, M., 2015. New streams and springs after the 2014 Mw6.0 South Napa earthquake.
585 Nature Communications, 6: 7597. DOI:10.1038/ncomms8597
586 Wang, C.-Y., Wang, C.-H., Manga, M., 2004. Coseismic release of water from mountains: Evidence
587 from the 1999 (Mw = 7.5) Chi-Chi, Taiwan, earthquake. Geology, 32(9): 769-772.
588 DOI:10.1130/g20753.1
589 Wang, S. et al., 2019. Changes in Groundwater Level Possibly Encourage Shallow Earthquakes in
590 Central Australia: The 2016 Petermann Ranges Earthquake. Geophysical Research Letters, 46(6):
591 3189-3198. DOI:10.1029/2018gl080510
592 Weingarten, M., Ge, S., 2014. Insights into water level response to seismic waves: A 24 year high-
593 fidelity record of global seismicity at Devils Hole. Geophysical Research Letters, 41(1): 74-80.
594 DOI:10.1002/2013gl058418
595 Zeng, X. et al., 2016. Comparison of microbial communities inside and outside of a denitrification
596 hotspot in confined groundwater. International Biodeterioration & Biodegradation, 114: 104-109.
597 DOI:10.1016/j.ibiod.2016.05.019
598
599
600

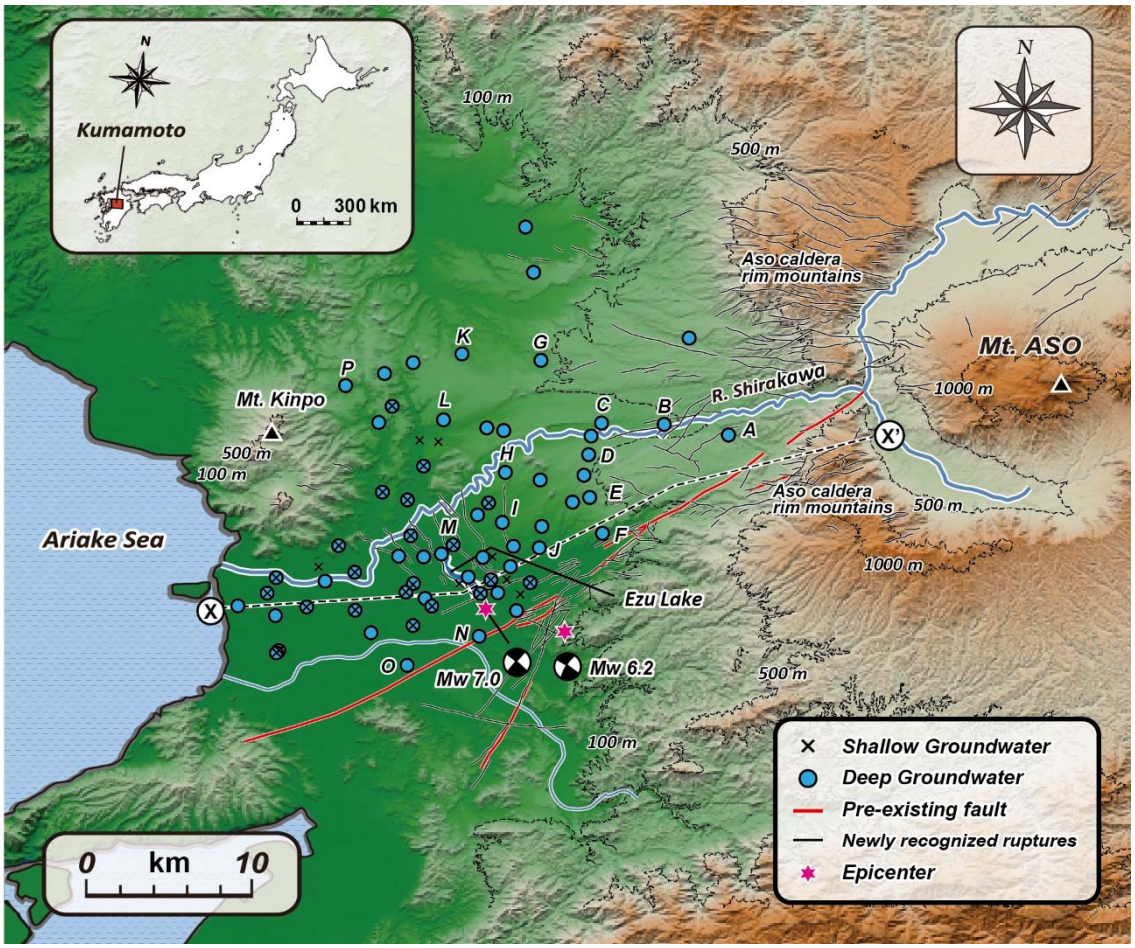

601

602 Fig. 1. Locations of groundwater level monitoring wells. At some sites, two wells are in one place for
603 confined and unconfined aquifer monitoring (cross inside open circle). Hydrogeological cross sections
604 X-X' is shown in Fig. 11.

605

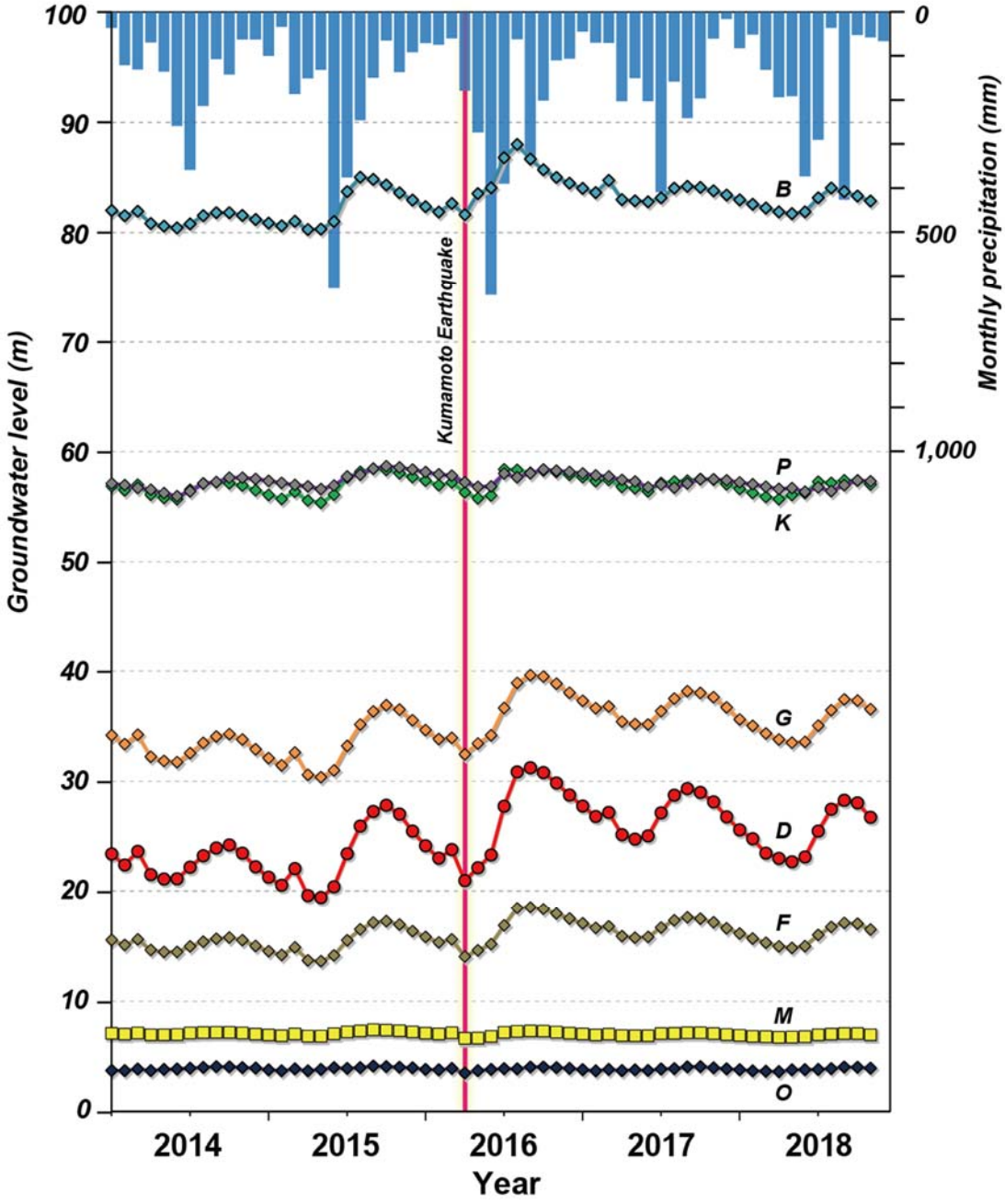

606

607 Fig. 2. Comprehensive monthly groundwater level fluctuation in Kumamoto area. The well location
608 number is corresponding to Fig. 1.

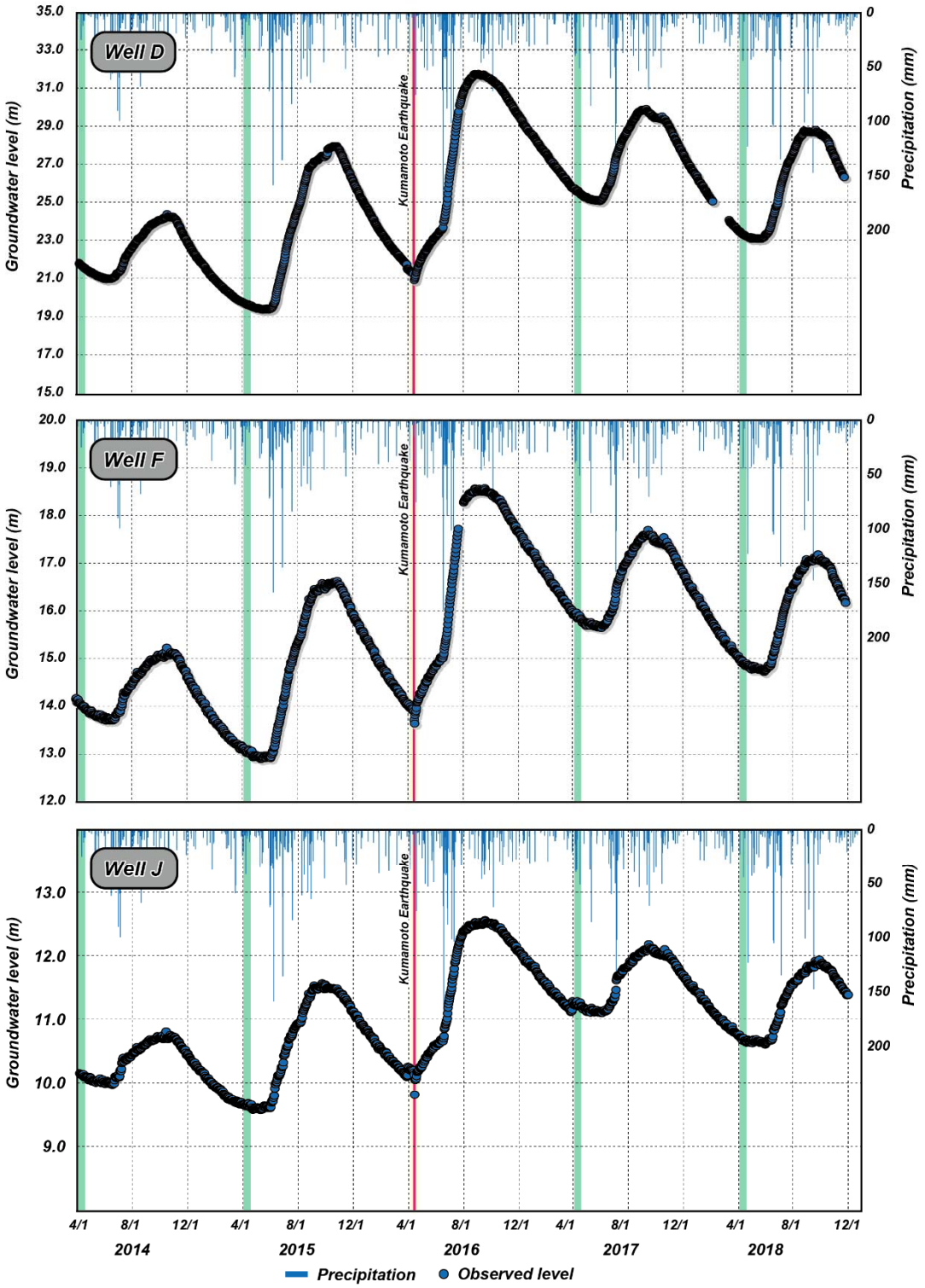

609

610 Fig. 3. Daily groundwater fluctuation before and after 2016 Kumamoto earthquake in some
611 observation wells (Wells D, F and J). Vertical green lines represent every April, the same month as the
612 earthquake occurred.

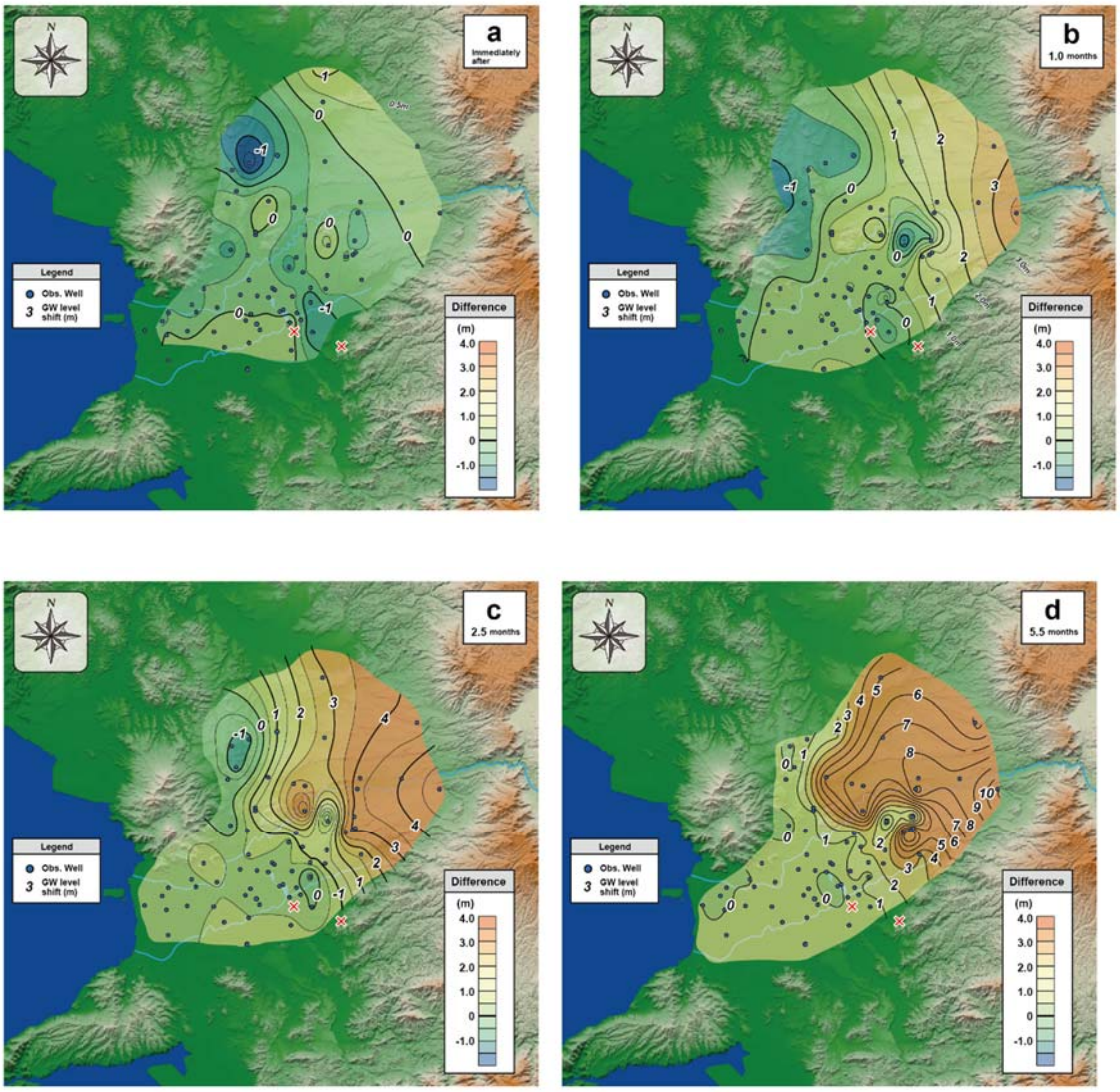

Fig. 4. Comparison of the groundwater levels of the second aquifer between before the occurrence of the earthquake (April 1, 2016) and water levels at different time after the earthquake: a) immediately (April 17, 2016), b) 1 month (May 15, 2016), c) 2.5 months (July 1, 2016), and d) 5.5 months (October 1, 2016) after the main shock.

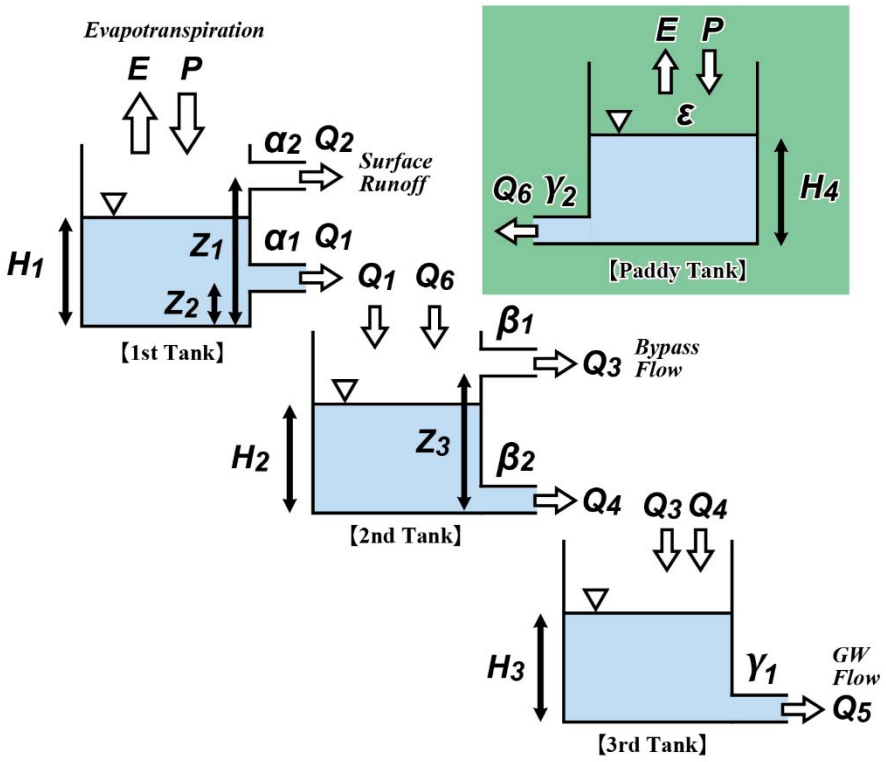

619

620 Fig. 5. Tank model configuration in this study. Seasonally added tank expresses groundwater recharge
621 from paddy field.

622

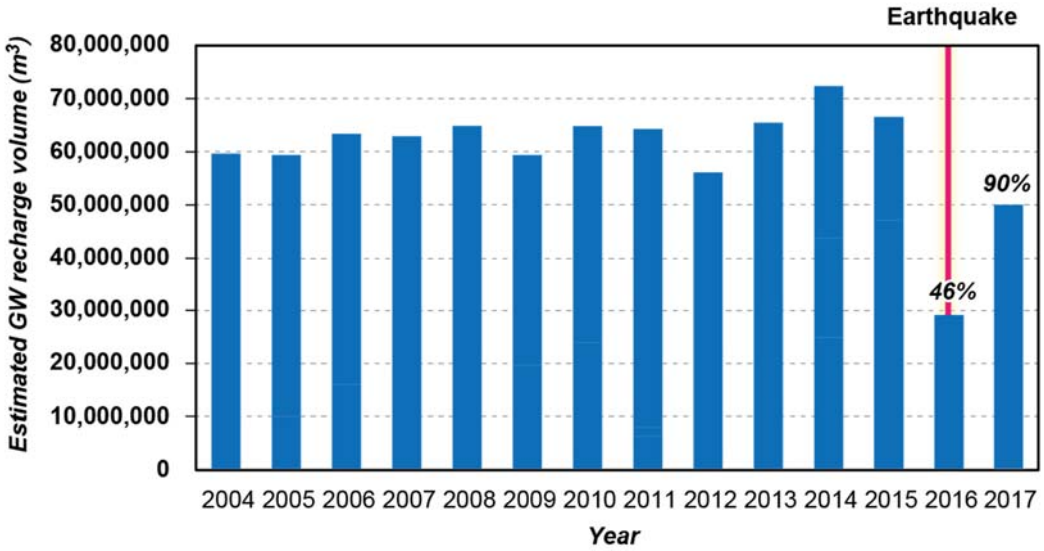

623

624 Fig. 6. Groundwater recharge from paddy fields. Recharge volume decreased because of damage to
625 the irrigation channels associated with the earthquake and water leakage because of earthquake
626 fractures that occurred in the paddy field area. This decreased volume (2016, 46%; 2017, 90%) adopted
627 when calculating groundwater level after the earthquake.

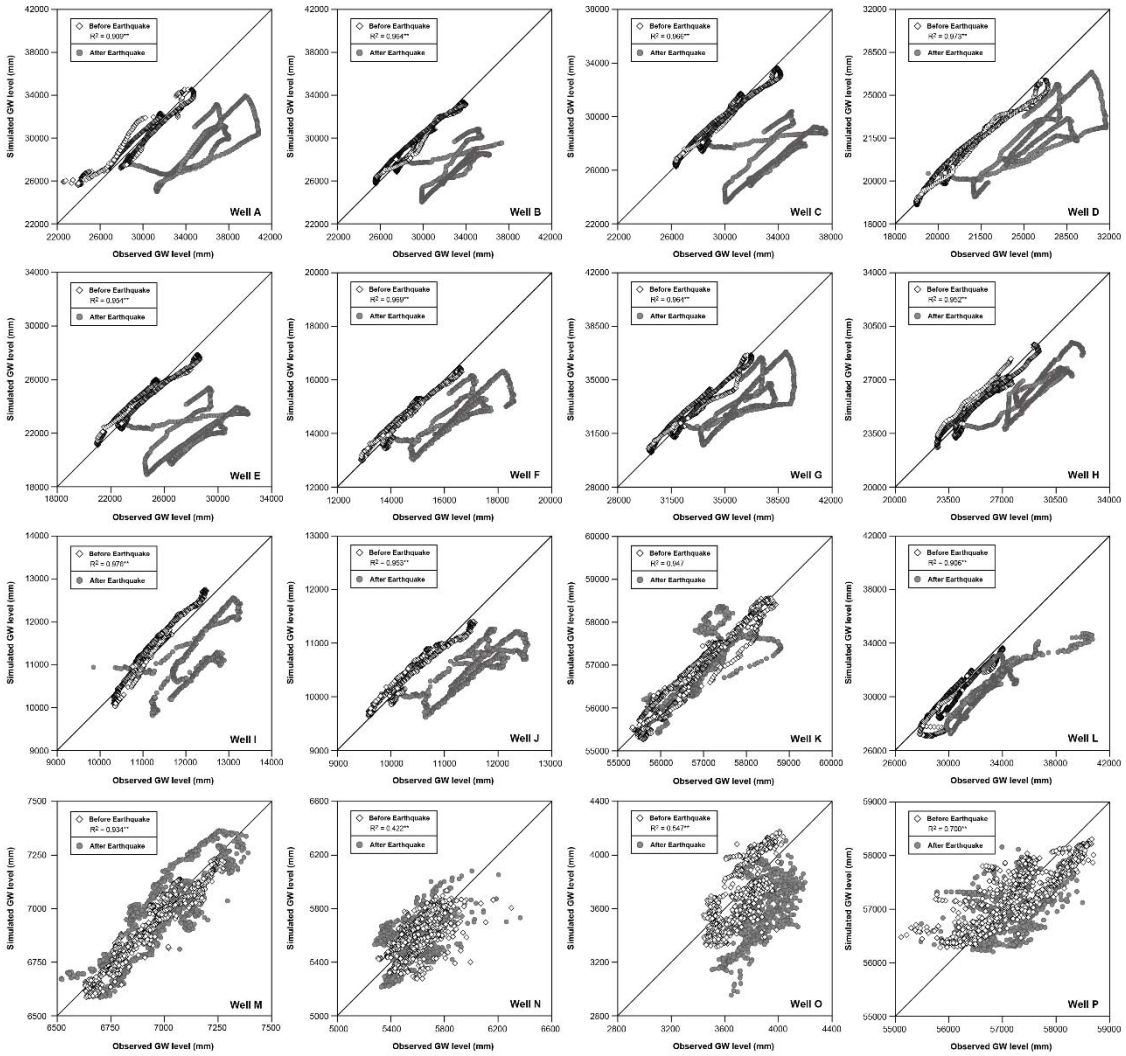

Fig.7. Scatter plot for the observed versus simulated groundwater level for 16 wells. Simulated groundwater level divided into two plots; Two years preceding the earthquake (Before Earthquake: from April 1, 2014 to April 15, 2016) and after main shock (After Earthquake: from April 16, 2016 to November 30, 2018). R^2 and ** represents the coefficient of determination and P value < 0.005, respectively.

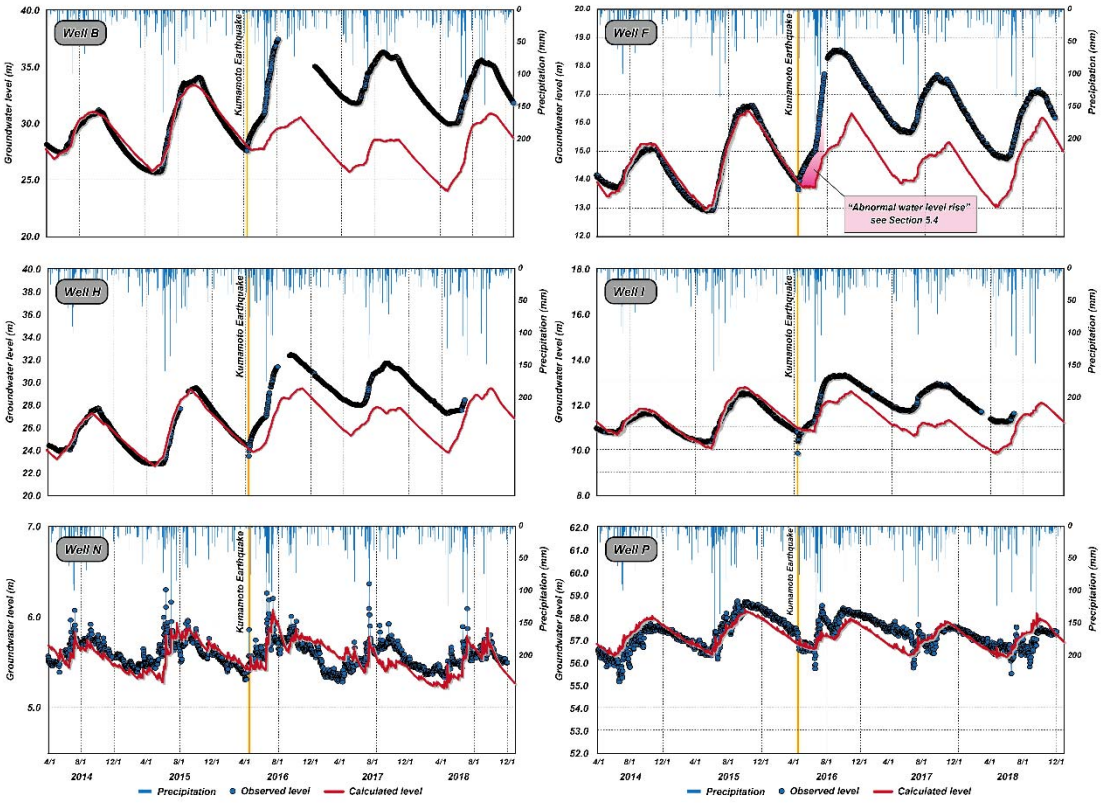

634

635 Fig. 8. Groundwater level fluctuation of observed (blue circle) and calculated using tank model (red
636 line) in some wells (Well B, F, H, J, N and P). The “abnormal water rise” shown in Well F is explained
637 in Section 5.4.

638

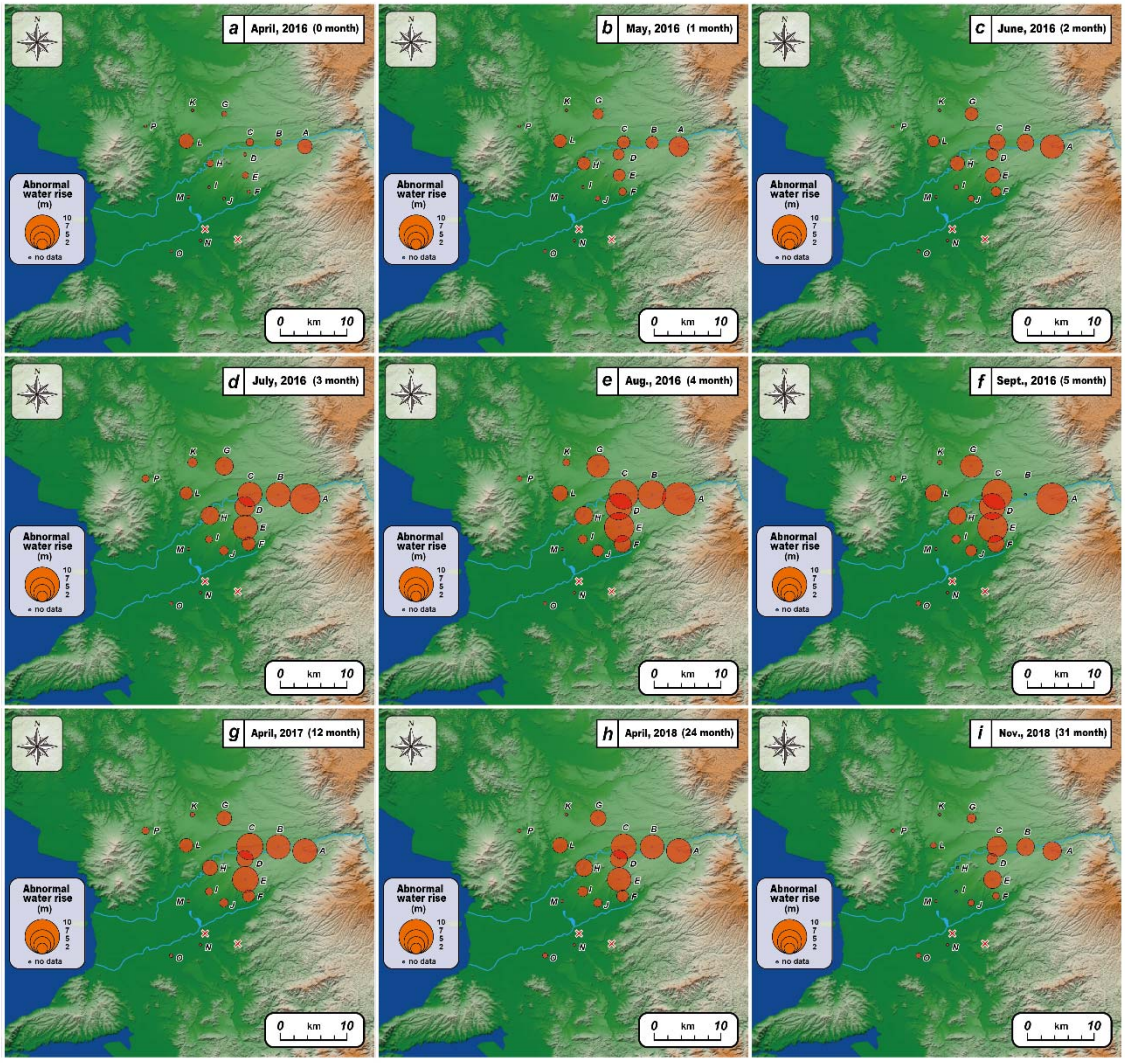

639

640 Fig. 9. The distribution map of the "abnormal water rise" in each nine period: a) April, 2016
641 (immediately after the earthquake), b) May, 2016 (1 month after), c) June, 2016 (2 month after), d)
642 July, 2016 (3 month after), e) August, 2016 (4 month after), f) September, 2016 (5 month after), g)
643 April, 2017 (12 month after), h) April, 2018 (24 month after) and i) November, 2018 (31 month after).

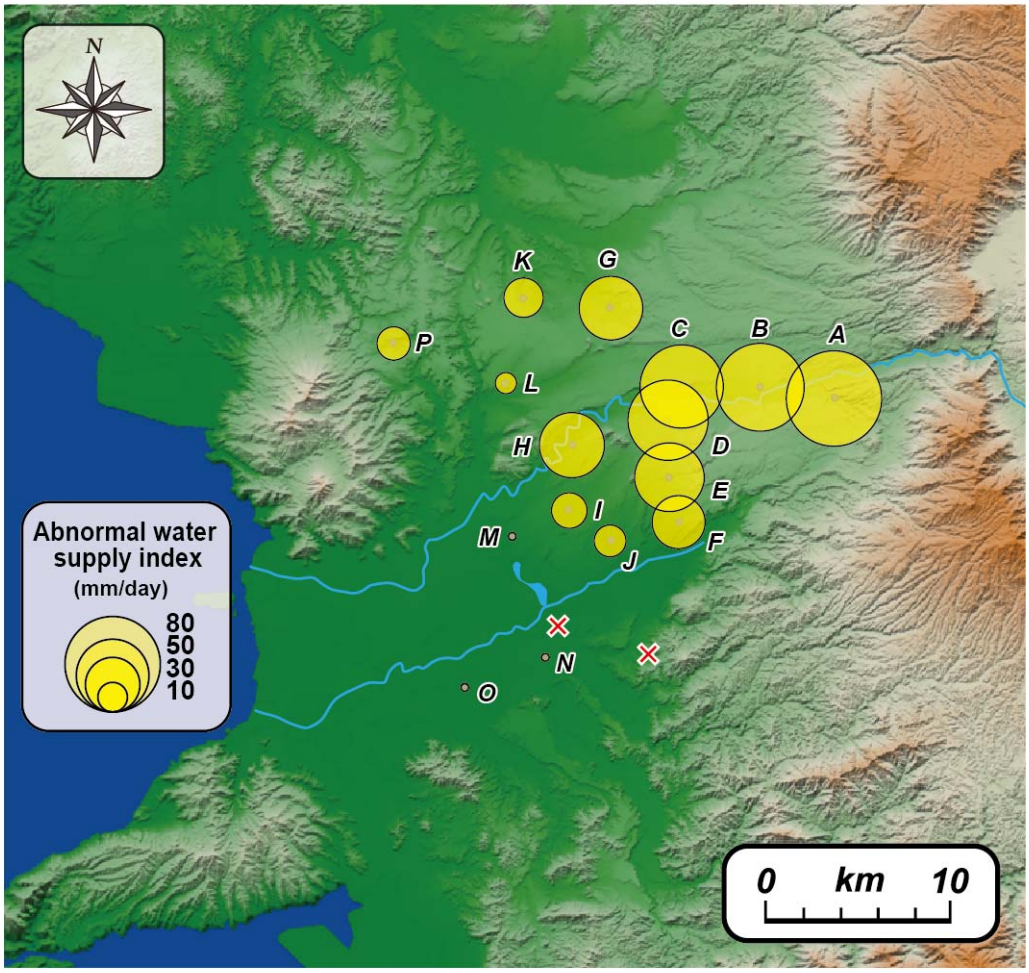

644

645 Fig. 10. Distribution of an “Abnormal water supply index”. A larger index implies new groundwater
646 supply occurred accompanying the earthquake.

647

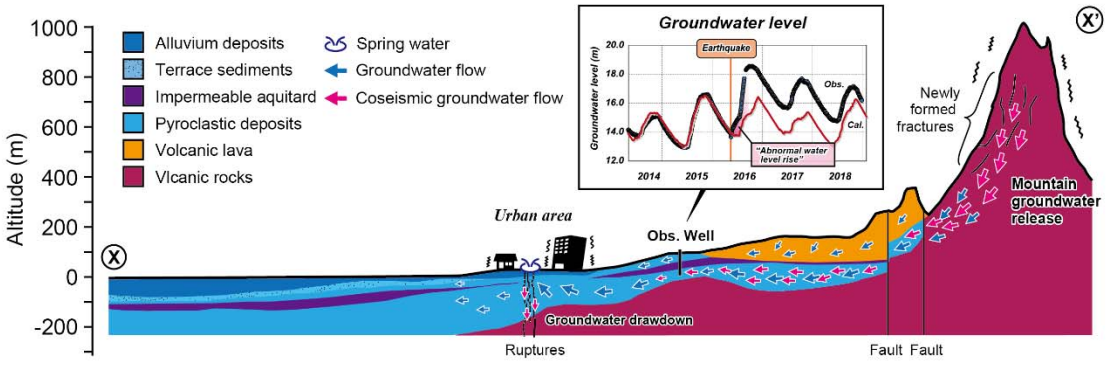

648

649 Fig. 11 Cartoon showing coseismic groundwater flow system changes. Location of the cross sections
650 X-X’ is shown in Fig. 1. Groundwater drawdown model in the urban area is after Hosono et al. (2019).

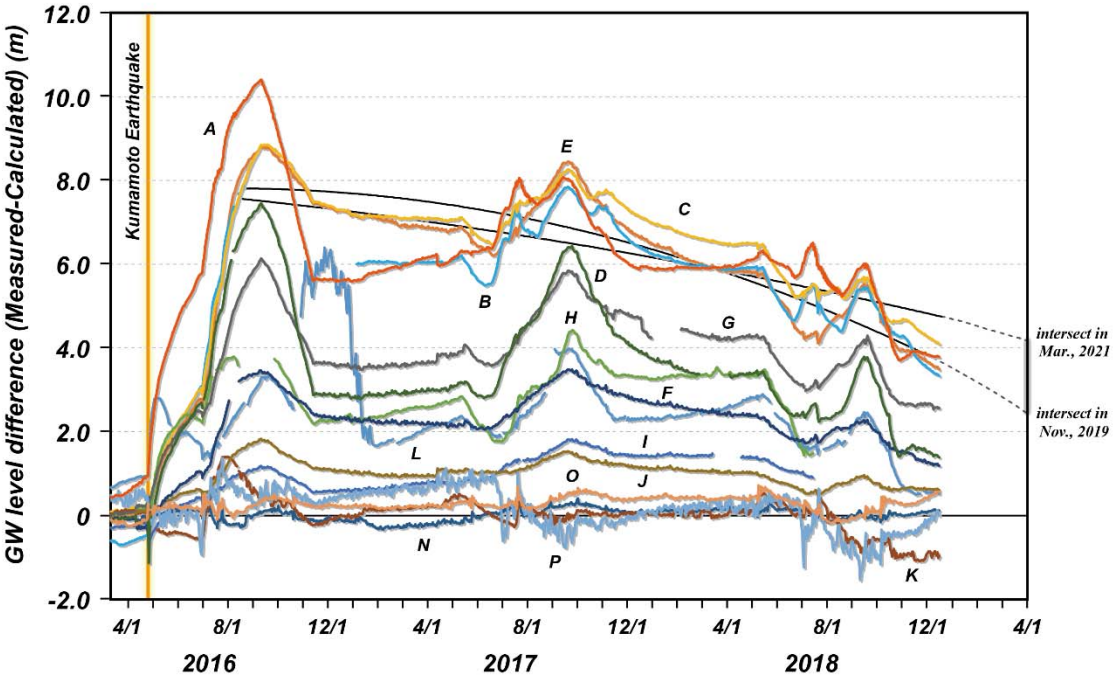

Fig. 12. Duration of abnormal water level in each observation well until two and a half years after the earthquake. The regression lines in polynomial curve for well A and E estimate the end date of the "abnormal water rise" (See 5.6 and Table 1).

Table 1. The estimated end date of the abnormal water level in Wells A to G. The end date was estimated by the regression curves of the water level reduction trend which obtained from August 2016 to the end of November 2018.

Well No.	The end date of the abnormal water level
A	March, 2021
B	November, 2019
C	January, 2020
D	January, 2020
E	November, 2019
F	November, 2019
G	December, 2019